

Cavitating Inducers

In the presence of cavitation, the transfer function for a pump or inducer will be considerably more complicated than that of equation (Nrp2). Even at low frequencies, the values of TP_{11} will become different from unity, because the head rise will change with the inlet total pressure, as manifest by the nonzero value of $d(\Delta p^T)/dp_1^T$ at a given mass flow rate, m_1 . Furthermore, the volume of cavitation, $V_C(p_1^T, m_1)$, will vary with both the inlet total pressure, p_1^T (or $NPSH$ or cavitation number), and with the mass flow rate, m_1 (or with angle of incidence), so that

$$[TP] = \begin{bmatrix} 1 + \frac{d(\Delta p^T)}{dp_1^T} \Big|_{m_1} & \frac{d\Delta p^T}{dm_1} \Big|_{p_1^T} \\ j\omega\rho_L \frac{dV_C}{dp_1^T} \Big|_{m_1} & 1 + j\omega\rho_L \frac{dV_C}{dm_1} \Big|_{p_1^T} \end{bmatrix} \quad (\text{Nrq1})$$

Brennen and Acosta (1973, 1975, 1976) identified this quasistatic or low frequency form for the transfer

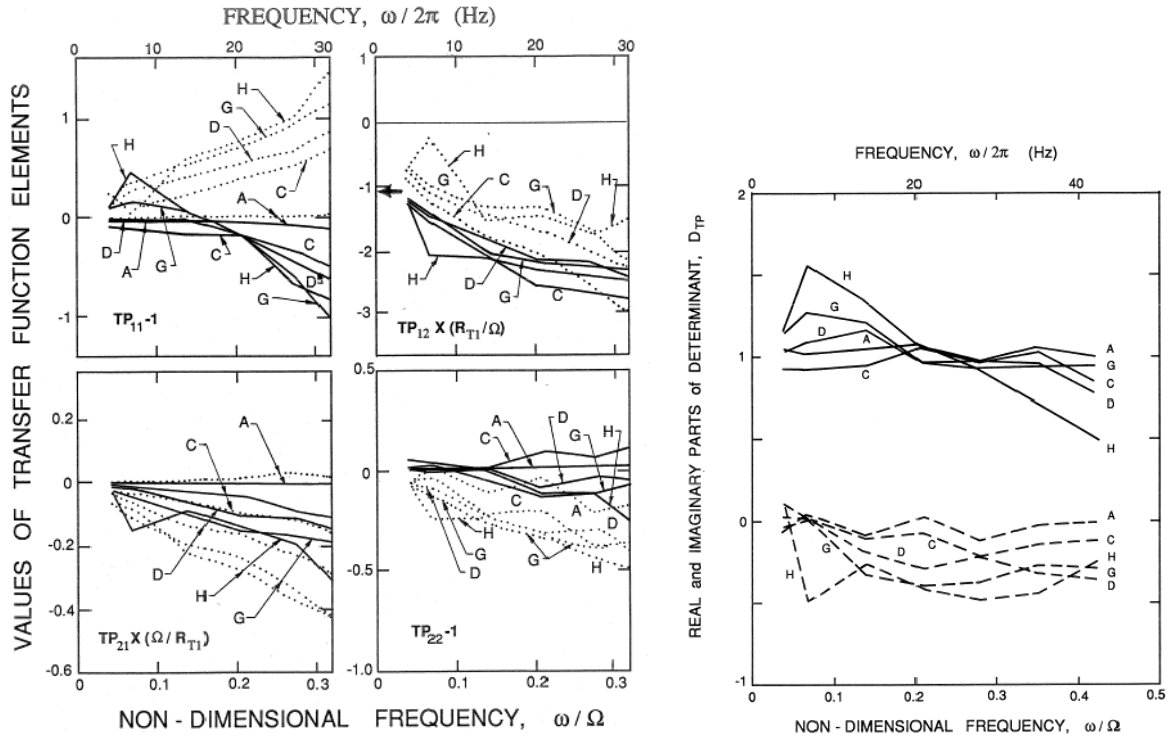


Figure 1: Left: Typical transfer functions for a cavitating inducer obtained by Brennen *et al.* (1982) for a 10.2 cm diameter inducer (Impeller VI) operating at 6000 rpm and a flow coefficient of $\phi_1 = 0.07$. Data is shown for four different cavitation numbers, $\sigma =$ (A) 0.37, (C) 0.10, (D) 0.069, (G) 0.052 and (H) 0.044. Real and imaginary parts are denoted by the solid and dashed lines respectively. The quasistatic pump resistance is indicated by the arrow (adapted from Brennen *et al.* 1982). Right: The determinants, D_{TP} , of the experimental transfer functions.

function of a cavitating pump, and calculated values of the cavitation compliance, $-\rho_L(dV_C/dp_1^T)_{m_1}$ and the cavitation mass flow gain factor, $-\rho_L(dV_C/dm_1)_{p_1^T}$, using the cavitating cascade solution discussed in the Section (Mbeu) on “Partially Cavitating Cascades”. Both the upper limit of frequency at which this quasistatic approach is valid and the form of the transfer function above this limit cannot readily be determined except by experiment. Though it was clear that experimental measurements of the dynamic transfer

functions were required, these early investigations of Brennen and Acosta did highlight the importance of both the compliance and the mass flow gain factor in determining the stability of systems with cavitating pumps.

Ng and Brennen (1978) and Brennen *et al.* (1982) conducted the first experiments to measure the complete transfer function for cavitating inducers. Typical transfer functions are those for the 10.2 *cm* diameter Impeller VI (see the section (Mbbi)), whose noncavitating steady state performance was presented in section (Mben). Transfer matrices for that inducer are presented in figure 1 as a function of frequency (up to 32 *Hz*), for a speed of 6000 *rpm*, a flow coefficient $\phi_1 = 0.07$ and for five different cavitation numbers ranging from data set A that was taken under noncavitating conditions, to data set C that showed a little cavitation, to data set H that was close to breakdown. The real and imaginary parts are represented by the solid and dashed lines, respectively. Note, first, that, in the absence of cavitation (Case A), the transfer function is fairly close to the anticipated form of equation (Nrp2) in which $TP_{11} = TP_{22} = 1$, $TP_{21} = 0$. Also, the impedance (TP_{12}) is comprised of an expected inertance (the imaginary part of TP_{12} is linear in frequency) and a resistance (real part of $-TP_{12}$) which is consistent with the quasistatic resistance from the slope of the head rise characteristic (shown by the arrow in figure 1 at $TP_{12}R_{T1}/\Omega = 1.07$). The resistance appears to increase with increasing frequency, a trend which is consistent with the centrifugal pump measurements of Anderson, Blade and Stevans (1971) which were presented in section (Nrp). The change in the resistance with frequency is not surprising since the resistance is some linear approximation to frictional effects that are not linear with flow-rate and may be closer to quadratic with the flow rate though, in the more general field of fluid mechanics, there are many different functional dependencies with flow-rate such as the square-root of flow-rate.

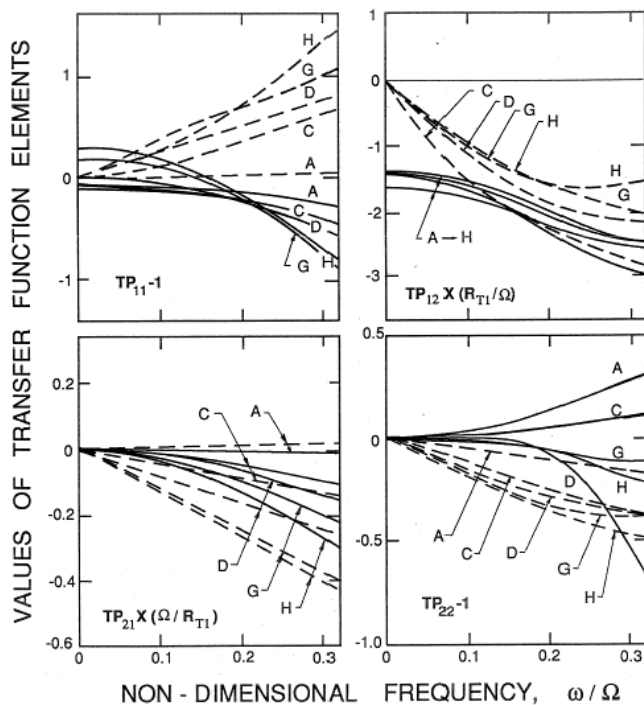


Figure 2: Polynomial curves fitted to the experimental data of figure 1 (adapted from Brennen *et al.* 1982).

It is also clear from figure 1 that, as the cavitation develops, the transfer function departs significantly from the form of equation (Nrp2). One observes that TP_{11} and TP_{22} depart from unity, and develop nonzero imaginary parts that are fairly linear with frequency. Also TP_{21} becomes nonzero, and, in particular, exhibits a compliance which clearly increases with decreasing cavitation number. All of these changes

mean that the determinant, D_{TP} , departs from unity as the cavitation becomes more extensive as shown in figure 1 (right). Note that $D_{TP} \approx 1$ for the non-cavitating case A, but that it progressively deviates from unity as the cavitation increases. We can conclude that the presence of cavitation can cause a pump to assume potentially active dynamic characteristics when it would otherwise be dynamically passive.

Polynomials of the form

$$TP_{ij} = \sum_{n=0}^{n^*} A_{nij}(j\omega)^n \quad (\text{Nr}q2)$$

were fitted to the experimental transfer function data using values of n^* of 3 or 5. To illustrate the result of such curve fitting we include figure 2, which depicts the result of curve fitting figure 1.

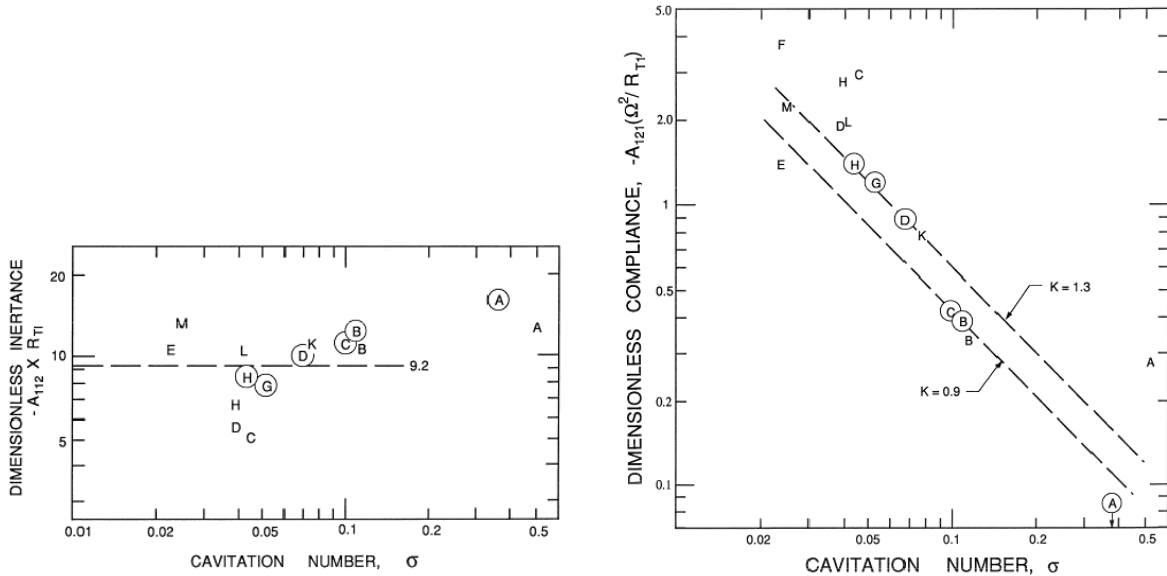


Figure 3: Left: The inertance, $-A_{112}$, non-dimensionalized as $-A_{112}R_{T1}$. Right: The compliance, $-A_{121}$, nondimensionalized as $-A_{121}\Omega^2/R_{T1}$. As functions of cavitation number for two axial inducer pumps (Impellers IV and VI) with the same geometry but different diameters. Data for the 10.2 cm diameter Impeller VI is circled and was obtained from the data of figure 1. The uncircled points are for the 7.58 cm diameter Impeller IV. Adapted from Brennen *et al.* (1982).

We now proceed to examine several of the coefficients A_{nij} that are of particular interest (note that $A_{011} = A_{022} = 1$, $A_{021} = 0$ for reasons described earlier). We begin with the inertance, $-A_{112}$, which is presented nondimensionally in figure 3 (left). Though there is significant scatter at the lower cavitation numbers, the two different sizes of inducer pump appear to yield similar dimensionless inertances. Moreover, the data suggest some decrease in the inertance with decreasing σ . On the other hand, the corresponding data for the compliance, $-A_{121}$, which is presented in figure 3 (right) seems roughly inversely proportional to the cavitation number. And the same is true for both the mass flow gain factor, $-A_{122}$, and the coefficient that defines the slope of the imaginary part of TP_{11} , A_{111} ; these are presented in figure 4. All of these data appear to conform to the physical scaling implicit in the nondimensionalization of each of the dynamic characteristics.

A more complete collection of the available data on the compliance and the mass flow gain factor for cavitating pumps is shown in figure 5 where those quantities are plotted against the cavitation number. The data on the SSME inducers in water is extracted from figures 3 and 4 while the J2 oxidizer data was

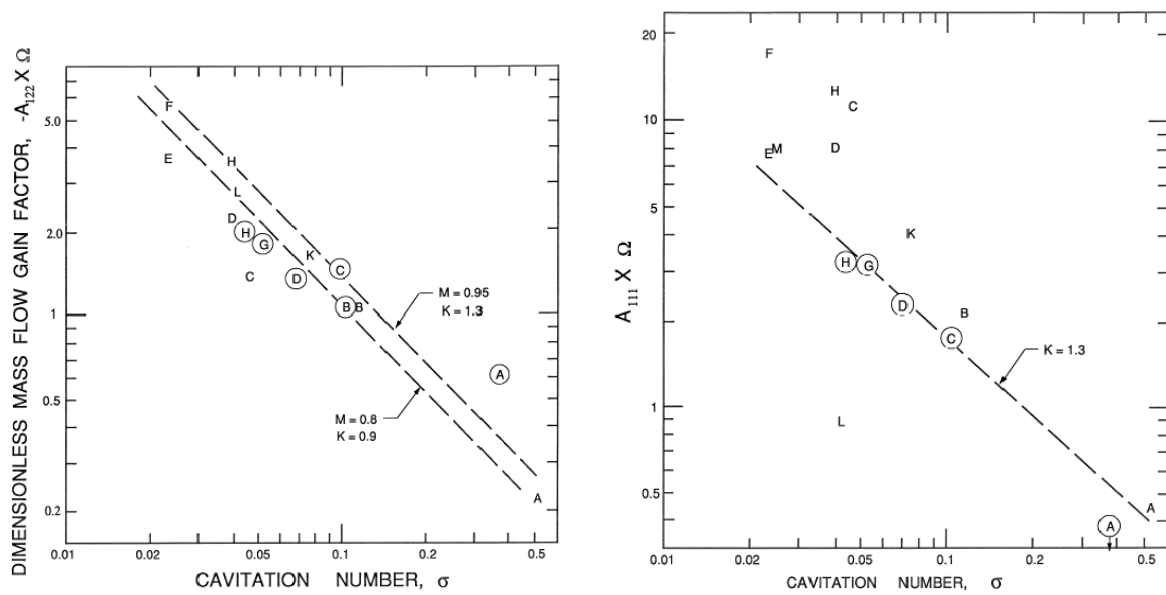


Figure 4: Left: The mass flow gain factor, $-A_{122}$, nondimensionalized as $-A_{122}\Omega$. Right: The characteristic, A_{111} , nondimensionalized as $A_{111}\Omega$. For the same circumstances as described in figure 3.

derived by Brennen and Acosta (1976) using test data and a heuristic dynamic model of the test facility. The LE-7 test data in liquid nitrogen was obtained by Shimura (1995). The LE-7A data is the only LOX data and was extracted from test data by Hori and Brennen (2011). All of this data is subject to significant uncertainty though the original SSME data is probably the most reliable since it is based on measurements of the complete dynamic transfer function. Nevertheless, with one exception, both the compliance and mass flow gain factor data exhibit significant consistency in which both C and M are inversely proportional to σ . The exception is the LE-7A LOX data for the mass flow gain factor; whether this discrepancy is within the uncertainty band or an actual LOX thermal effect remains to be determined.

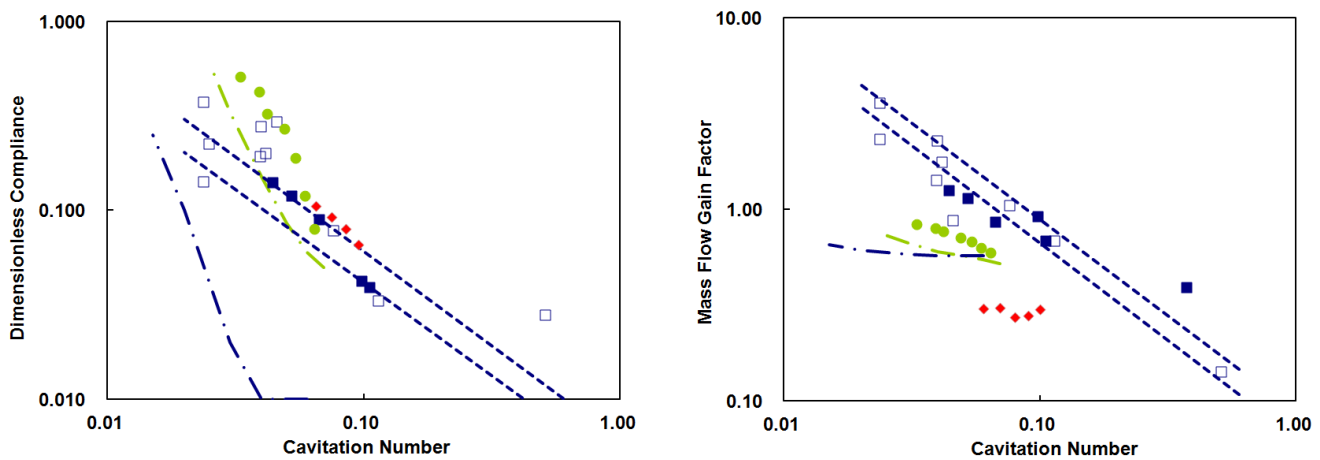


Figure 5: Dimensionless cavitation compliance (left) and mass flow gain factor (right) plotted against tip cavitation number for: [a] Brennen *et al.* (1982) SSME 10.2cm model inducer in water (solid blue squares) [b] Brennen *et al.* (1982) SSME 7.6cm model inducer in water (open blue squares) [c] Brennen (1978) bubbly flow model results (dashed blue lines) [d] Brennen & Acosta (1976) SSME LPOTP blade cavitation prediction (dot-dash blue line) [e] Brennen & Acosta (1976) J2-Oxidizer data (solid green circles) [f] Brennen & Acosta (1976) J2-Oxidizer blade cavitation prediction (dot-dash green line) [g] Yonezawa *et al.* (2012) quasistatic CFD cascade data (solid red diamonds).

Figure 5 also includes predictions from the blade cavitation analysis of Brennen and Acosta (1976) which has the advantage that it does not contain any empirical parameter, as such. However, it assumes that all the cavitation is contained within a single cavity attached to each blade. Moreover the comparisons in figure 5 suggest that such a model does not yield very useful results which is not surprising when photographs of practical inducers show that the cavitation is primarily bubbly cavitation and not blade cavitation (Brennen 1994). Also included in figure 5 are several predictions from the bubbly flow model of Section (Nrt) (dashed blue lines for several choices of K' and M'). The predictions appear to provide a useful benchmark for future data evaluation and comparison. Also included in figure 5 are quasistatic compliances and mass flow gain factors recently derived by Yonezawa *et al* (2012) from steady CFD calculations of the cavitating flow in linear cascades. They also performed calculations at a series of flow coefficients that show a general trend of increasing compliance and mass flow gain factor as the flow coefficient is decreased.

Before further analysis, we digress briefly to review the non-dimensionalization of these results. Note that the fundamental variables in equation (Nr_q1) are the total pressure whose units are the $[kg/ms^2]$ and the mass flow rate with units of $[kg/s]$. Therefore the resistance, $-Re\{T_{12}\}$, has units of $[m^{-1}s^{-1}]$. The compliance, C , is defined as $C = -\rho_L(dV_C/dp_1^T)_{m_1}$ and therefore has units of $[ms^2]$. The units of T_{21} are $[ms]$ and the mass flow gain factor, $M = -\rho_L(dV_C/dp_1^T)_{m_1}$, are $[s]$. It is convenient to non-dimensionalize the total pressure using $\frac{1}{2}\rho_L U^2$ (where U is a blade tip velocity, at the inlet tip for pumps and the discharge tip for turbines) and the mass flow rate using $\rho_L U A$ where A is the cross-sectional area of the inlet or discharge. Using these dimensionless variables in the dimensionless transfer matrix it follows that

- the element T_{21} becomes $T_{21}U/2A$
- the element T_{22} becomes T_{22}
- the element T_{12} becomes $T_{12}2A/U$ and
- the resistance, $R = -Re\{T_{12}\}$, becomes non-dimensionalized as $2AR/U$

These are straightforward. However, complications arise because there are two different possible ways to non-dimensionalize the frequency, ω , and both have their merits:

[A] The first possibility is to define a dimensionless frequency, $\omega' = \omega h/U$ where h is the blade tip spacing, $h = \pi D/Z$ where Z is the number of pump or turbine blades. This choice recognizes the blade passage frequency, U/h , as the key inherent frequency of the flow. It has the property that it ascribes a cavitation volume to each blade; hence the key difference between this choice and choice [B] is the appearance of the number of blades, Z , in ω' . This non-dimensional frequency emerges naturally in the blade cavitation analysis of Brennen and Acosta (1973) and in the bubbly flow model of Section (Nrt).

[B] A second possible choice is $\omega'' = \omega/\Omega$ where Ω is the radian rotation rate in radians/sec. This has the advantage of simplicity and may be more appropriate in turbomachines that manifest a cavitation volume that is independent of the individual blades; such might be case, for example, with a single draft tube vortex in a turbine.

With the first non-dimensional frequency, ω' , the dimensionless compliance denoted by C' and the dimensionless mass flow gain factor denoted by M' become

$$\omega' C' = \omega C \quad \text{and} \quad \omega' M' = \omega M \quad (\text{Nr}_q3)$$

so that

$$C' = CZ\Omega^2/2\pi^2 D \quad \text{and} \quad M' = MZ\Omega/2\pi \quad (\text{Nr}_q4)$$

With this first scheme the pump and turbine compliances, C' , are as shown in Figures 3 and 5 while the pump mass flow gain factors, M' , are as shown in Figures 4 and 5.

With the second non-dimensional frequency, ω'' , the dimensionless compliance, C'' , and the dimensionless mass flow gain factor, M'' , become

$$\omega'' C'' = \omega C' \quad \text{and} \quad \omega'' M'' = \omega M' \quad (\text{Nr}q5)$$

so that

$$C'' = C' \Omega^2 / 2\pi^2 D \quad \text{and} \quad M'' = M' \Omega \quad (\text{Nr}q6)$$

With this second scheme the pump and turbine compliances, C'' , and mass flow gain factors, M'' , are as shown in Figure 6. It appears that the second non-dimensional frequency scheme does a better job

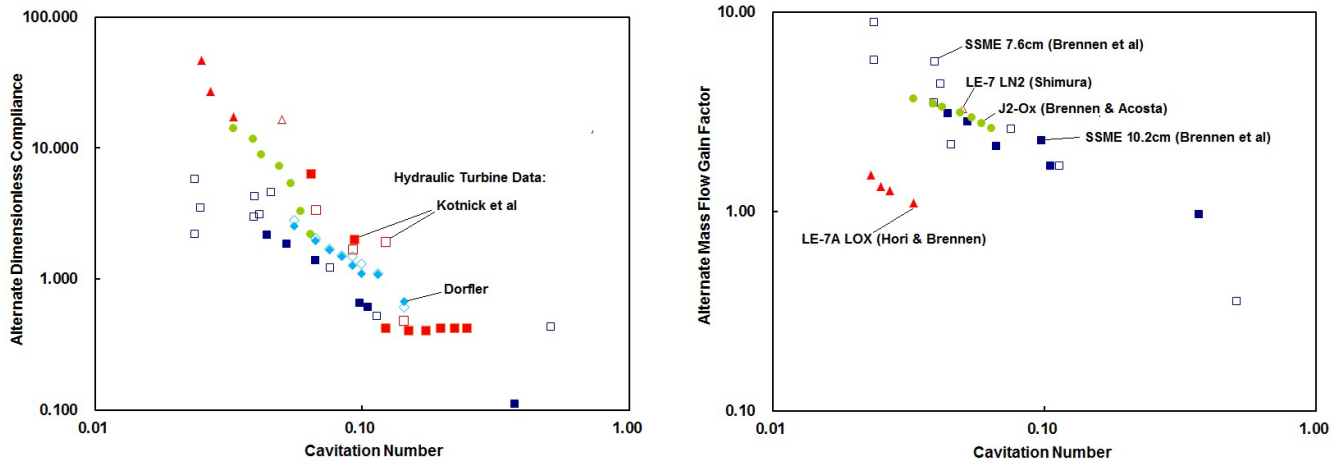


Figure 6: The dimensionless compliance, C'' (left), and mass flow gain factor, M'' (right), plotted versus the cavitation number, σ , for many inducer pumps. Also plotted is data from Dorfler (2018) and Manderla *et al.* (2016) for Francis turbines.

of collapsing the turbine data onto the pump data but whether this is significant or merely coincidental remains to be seen.